Iraqi Journal of Science, 2025, Vol. 66, No. 3, pp: 970-991
DOI: 10.24996/ijs.2025.66.3.1

ISSN: 0067-2904

Synthesis and Characterization of New 7-Chloroisatin Derivatives and Study of Their Potential Antioxidant Activity

Mohammed G.A. Al-Khuzaie[1]*, Masar J. Al-Kurdy[2], Suaad M.H. Al-Majidi[3]
[1]*Department of Nursing Techniques, Technical Institute of Al-Diwaniyah, AL-Furat AL-Awsat Technical University (ATU), Al-Diwaniyah, Iraq*
[2] *Department of Community health Techniques, Technical Institute of Al-Diwaniyah, AL-Furat AL-Awsat Technical University (ATU), Al-Diwaniyah, Iraq*
[3]*Department of Chemistry, College of Science, University of Baghdad, Baghdad, Iraq*

Received: 5/9/2023 Accepted: 20/3/2024 Published: 30/3/2025

Abstract

A series of novel spiro azetidine and thioazetidine scaffolds incorporating an isatin subunit were successfully synthesized. The protocol involved reacting Schiff base derivatives of 7-chloroisatin with phenyl isocyanate or phenyl thioisocyanate. The new derivatives were obtained in excellent yield and characterized by different techniques such as FTIR, HNMR and ^{13}CNMR. Furthermore, *in silico*, *in vitro*, and *in vivo* investigations were performed to assess the bioactivity of prepared compounds as antioxidants. The *in-silico* analysis encompassed the evaluation of pharmacokinetic and pharmacodynamic properties for all compounds, revealing favorable characteristics. Subsequently, molecular docking studies were performed with two proteins: VEGFR-2 and ALR2. The results demonstrated good docking scores for compounds **1-4**. The *in vitro* assessments involved the evaluation of the potential antioxidant activity of all compounds using two methods: the total antioxidant capacity method and the DPPH scavenging activity method. The results demonstrated that all compounds exhibited noteworthy to excellent antioxidant activity. Based on these findings, compound **2** was selected for further investigation in the *in vivo* study using rats. In the *in vivo* experiment, male rats were administered a dose of 200 mg/0.5ml DMSO/rat/ day of compound **2** for 4-weeks, and the concentrations of total antioxidant capacity and MDA in their serum were measured. The results indicated that compound **2** exhibited commendable performance as an antioxidant agent.

Keywords: Isatin, Azetidine, Antioxidant, Molecular docking.

تخليق و تشخيص مشتقات جديدة من 7-كلورواياساتين و دراسة فعاليتها المحتملة كمضادات اكسدة

محمد غانم عباس الخزاعي[1]*, مسار جبار جري الكردي[2], سعاد محمد حسين الماجدي[3]
[1]قسم تقنيات التمريض, المعهد التقني، الديوانية, جامعة الفرات الاوسط التقنية, الديوانية, العراق
[2]قسم تقنيات صحة المجتمع, المعهد التقني،الديوانية, جامعة الفرات الاوسط التقنية, الديوانية, العراق
[3]قسم الكيمياء, كلية العلوم, جامعة بغداد, بغداد, العراق

* Email: mohammed.alkhuzaie@atu.edu.iq

الخلاصة

سلاسل من جزيئات سبايرو ازيتيدين وثايوازيتيدين النشطة حيويًا تحتوي على وحدة الإيساتين تم تحضيرها عن طريق تفاعل مشتقات قواعد شيف من 7-كلوروإيساتين مع فنيل أيزوسيانات وفنيل ثايوأيزوسيانات على التوالي. تم الحصول على المشتقات الجديدة بنسبة منتوج ممتازة و تم تشخيصها باستخدام تقنيات مختلفة مثل FTIR و HNMR و ^{13}CNMR. علاوة على ذلك، تم إجراء دراسات النظرية و المختبرية والحيوية لتقييم النشاط الحيوي للمركبات المحضرة كمضادات الأكسدة. شمل التحليل النظري تقييم الخصائص الدوائية الحرارية و الحركية لجميع المركبات ، و اظهرت جميعها خصائص مناسبة. بعد ذلك، تم إجراء دراسات التشابك الجزيئي مع بروتينين: VEGFR-2 و ALR2. أظهرت النتائج نتائج تشابك جيدة للمركبات **1-4**. شملت الدراسة المختبرية تقييم النشاط المحتمل كمضادات الأكسدة لجميع المركبات باستخدام طريقتين: طريقة السعة الكلية المضادة للأكسدة و طريقة فعالية كسح الDPPH. أظهرت النتائج أن جميع المركبات أظهرت نشاطًا ممتازًا أو ملحوظًا كمضادات الأكسدة. استنادًا إلى هذه النتائج، تم اختيار المركب **2** لدراسة تأثيره في الجسم الحي باستخدام الجرذان. تضمنت التجربة الحيوية إعطاء ذكور الجرذان جرعة 200 مجم / 0.5 مل DMSO / جرذ / يوم من المركب **2** لمدة 4-أسابيع، وتم قياس تراكيز السعة الكلية لمضادات الأكسدة ومادة MDA في مصل الدم. أشارت النتائج إلى أن المركب **2** أظهر أداءً ممتازًا كعامل مضاد للأكسدة.

1. Introduction

The human body naturally generates a diverse array of reactive oxygen species (ROS), also known as oxygen radicals, through metabolic processes. This includes single oxygen, hydrogen peroxide, superoxide, and hydroxyl radicals [1, 2]. ROS fulfill crucial physiological functions like protein-mediated immunity, programmed cell death (apoptosis), transcription factor activation via phosphorylation, and cellular differentiation. However, ROS production and accumulation must be tightly regulated at low levels within cells to avoid oxidative damage. This is achieved through concerted antioxidant defenses involving both enzymatic and non-enzymatic inhibitors [3]. There are other ways in which ROS can be produced and increase its concentration in the body, such as radiation exposure, smoking, and medications[4]. An increase in the concentration of ROS in the body causes an imbalance state between them and antioxidants, called oxidative stress. ROS increasement could have harmful effects on important cellular structures such as lipids, proteins, and nucleic acids. There is ample evidence that oxidative stress may be responsible to varying degrees for the onset and/or progression of various diseases (e.g., cancer, diabetes, metabolic disorders, atherosclerosis, and cardiovascular disease)[5].

The global trend in the treatment of oxidative stress conditions is the use of antioxidants synthesized from biologically active molecules. Isitine, a heterocyclic compound, is one of the most important biologically active compounds. It is found in mammalian tissues and fluids and is a metabolic byproduct of human adrenaline [6, 7]. Numerous isatin derivatives exhibit a range of biological activities, such as antimicrobial [8], antioxidant [9], anticancer [10], α-glucosidase inhibitor [11], and antitubulin agents [12]. In addition, it has been found that most isatin compounds may have antioxidant properties. Due to the N-H and C=O units in its lactam ring, isatin has the ability to scavenge free radicals [12, 13]. The indole ring, which is the main component of the isatin structure, is the main component of the drug sunitinib, which is used to treat cancer. Therefore, this structure has been increasingly studied in recent years [14]. Another biologically active indole compound is liorestat, a highly potent and selective aldose reductase (ALR2) inhibitor with excellent oral bioavailability [15]. Aldose reductase, a member of the aldoketo reductase superfamily, is the first and rate-determining enzyme of the polyol pathway. It catalyzes, especially in a hyperglycemic state,

the NADPH-dependent reduction of various carbonyl compounds, including glucose, producing sorbitol [16]. Abnormal activation of the polyol pathway is an important cause of oxidative stress. Under hyperglycemic conditions, more than 30% of glucose enters the aldose reductase-dependent polyol pathway, which consumes NADPH and consequently reduces glutathione levels (an intracellular antioxidant)[17]. Moreover, oxidative stress occurs during the conversion of sorbitol to fructose by sorbitol dehydrogenase, while the cofactor NAD^+ is converted to NADPH. The sharp decrease in NADPH and NAD^+ leads to changes in the redox potential in cells, which can lead to an increase in intracellular reactive oxygen species, ultimately resulting in cellular oxidative stress[18]. In addition, fructose is converted to fructose-3-phosphate and 3-deoxyglucosone, which are more potent non-enzymatic glycation agents. These agents increase the formation of advanced glycation end products, which eventually lead to the formation of ROS and oxidative stress[19]. Thus, aldose reductase enzyme inhibitors may indirectly inhibit oxidative stress. Therefore, the combination of direct antioxidant activity and ALR2 inhibition in the development of new multifunctional aldose reductase inhibitors may help to improve the efficacy of treatment.

Based on the reported evidence, new spiro-isatin derivatives were synthesized, which may exhibit potent antioxidant activity considering the known properties of isatin. The antioxidant activities of the synthesized compounds were studied *in vitro* by two tests (total antioxidant capacity assay and DPPH scavenging method) and using ascorbic acid as a standard, *in vivo* and *in silico*.

2. Chemicals and methods

BDH, Merck, Fluka, and Sigma Aldrich are the suppliers of all chemicals. An SMP3 melting point apparatus was used to measure the melting points, which were subsequently left uncorrected. Using a KBr disc in the spectral range (4000–600) cm^{-1}, FTIR spectra were examined with a SHIMAZU FTIR-8400 spectrophotometer. Using TMS as reference and DMSO-d_6 as solvent, ^{1}HNMR and ^{13}CNMR spectra were recorded with an ECA at 500 MHz. The UV-1900i spectrophotometer, Shimadzu, Japan, was used to record the UV-VIS spectra. TLC was performed for each compound prepared.

*2.1 Synthesis of 7-chloro-3-((4-aryl)imino)indolin-2-one (**1-4**)*[20]

Schiff bases of 7-chloroisatin were synthesized through a condensation reaction between substituted aromatic amines and 7-chloroisatin. In a typical procedure, 7-chloroisatin (1.0 g, 3.0 mmol) was dissolved in N,N-dimethylformamide (DMF, 5 mL) in a round bottom flask. To this was added the requisite aromatic amine (3.0 mmol) and a catalytic amount of glacial acetic acid (3 drops). The reaction mixture was heated at reflux for 10-12 hours to drive formation of the imine bond between the amine and carbonyl carbon of 7-chloroisatin. Upon completion, the mixture was cooled to room temperature and poured slowly into an ice water bath. This facilitated precipitation of the desired Schiff base product. The resulting solid was isolated through vacuum filtration, washed with water to remove residual reactants, then recrystallized from a suitable high boiling solvent.

*2.1.1 7-chloro-3-((4-chlorophenyl)imino)indolin-2-one (**1**)*

Yield= 83%, light brown, m.p.=125-127, FTIR (in KBr disk, 4000-400 cm^{-1}) ν N-H at 3215, aromatic νC-H at 3072, νC=O at 1726, ν C=N at 1676, ν C=C at 1618-1537, ν C-Cl at 742.

*2.1.2 7-chloro-3-((4-(dimethylamino)phenyl)imino)indolin-2-one (**2**)*

Yield= 90%, Black, m.p.= 130-132, FTIR (in KBr disk, 4000-400 cm^{-1}) n N-H at 3238, aromatic νC-H, ν -C-H at 2935, νC=O at 1718, ν C=N at 1670, ν C=C at 1610-1519, ν C-Cl at 748. ^{1}H NMR (400 MHz, DMSO-d6) δ 2.95 ppm (s, 6H, N-CH_3), δ 6.59 – 8.14 ppm (m, C-H aromatic), δ 8.51 ppm (s, 1H, N-H).

*2.1.3 7-chloro-3-((4-nitrophenyl)imino)indolin-2-one (**3**)*

Yield= 95%, brown, m.p.= 166-168, FTIR (in KBr disk 4000-400 cm^{-1}) ν N-H at 3240 aromatic νC-H at 3083, νC=O at 1726, ν C=N at 1679, ν C=C at 1620-1596, ν NO_2 at 1475 asym, 1311 sym, ν C-Cl at 745. ^{1}HNMR (400 MHz, DMSO-d6) δ 6.00 - 8.23 ppm = (m, C-H aromatic), δ 8.70 ppm = (s, 1H, N-H). ^{13}C NMR (101 MHz, DMSO-d6) δ 155.6 ppm (C=O), δ 135.5 ppm (C=N), δ 128.8-104.5 ppm (CH aromatic).

*2.1.4 7-chloro-3-((4-hydroxyphenyl)imino)indolin-2-one (**4**)*

Yield= 88%, Deep-brown, m.p.=170-172 FTIR (in KBr disk, 4000-400 cm^{-1}) 3382, ν N-H at 3284, aromatic νC-H at 3090, νC=O at 1718, ν C=N at 1670, ν C=C at 1618-1505, ν C-O at 1085, ν C-Cl at 746. ^{1}HNMR (400 MHz, DMSO-d6) δ 6.72 – 8.34 ppm (m, C-H aromatic), δ 8.75 ppm (s, 1H, N-H), δ 8.93 ppm (s, 1H, O-H).

*2.2 Synthesis of 7'-chloro-1-(4-aryl)-3-phenylspiro[[1,3]diazetidine-2,3'-indoline]-2',4-dione (**5-8**)*[21]

A mixture was prepared by combining 3.27 mL of phenyl isocyanate (equivalent to 30.0 mmol) and Schiff base derivatives (1-4), also amounting to 30.0 mmol. This mixture was dissolved in 5 mL of Dimethylformamide (DMF). The solution was then heated under reflux for a period ranging from 20 to 23 hours. After this period, the reaction mixture was allowed to cool before being poured into a container filled with ice water. This caused a solid to precipitate out of the solution. This solid was collected by filtration, rinsed with water, and then recrystallized using an appropriate solvent.

*2.2.1 7'-chloro-1-(4-chlorophenyl)-3-phenylspiro[[1,3]diazetidine-2,3'-indoline]-2',4-dione (**5**)*

Yield= 71%, off white, m.p.=180-182 FTIR (in KBr disk, 4000-400 cm^{-1}) ν N-H at 3290, aromatic νC-H at 3035, νC=O at 1731, ν N-C=O at 1649, ν C=C at 1621-1595, ν C-Cl at 786. ^{13}C NMR (101 MHz, DMSO) δ 162.2 ppm (C=O), δ 152.4 ppm (N-(C=O)-N), δ139.6-106.1 ppm (CH aromatic) δ 102.7 ppm (N-C-N).

*2.2.2 7'-chloro-1-(4-(dimethylamino)phenyl)-3-phenylspiro[[1,3]diazetidine-2,3'-indoline]-2',4-dione (**6**)*

Yield= 76%, intense brown, m.p.= 183-185 FTIR (in KBr disk, 4000-400 cm^{-1}) νN-H at 3301, aromatic νC-H 3056, ν -C-H at 2927, νC=O at 1690, ν N-C=O at 1633, ν C=C at 1617-1596, ν C-Cl at 754. ^{1}H NMR (400 MHz, DMSO-d6) δ 3.01 (s, 6H, N-CH_3), δ 6.95 – 7.46 (m, C-H aromatic) ppm, δ 8.67 (s, 1H, N-H) ppm. ^{13}C NMR (101 MHz, DMSO) δ 161.1 ppm (C=O), δ 152.4 ppm (N-(C=O)-N), δ 148.7 ppm (C-N$(CH_3)_2$), δ 139.6-110.7 ppm (CH aromatic), δ 100.9 ppm (N-C-N), δ 51.4 ppm (N$(CH_3)_2$).

*2.2.3 7'-chloro-1-(4-nitrophenyl)-3-phenylspiro[[1,3]diazetidine-2,3'-indoline]-2',4-dione (**7**)*

Yield= 88%, Brown, m.p.= 160-162 FTIR (in KBr disk, 4000-400 cm^{-1}) νN-H at 3282, aromatic νC-H at 3064, νC=O at 1726, νN-C=O at 1668, ν C=C at 1619-1594, ν NO_2 at 1444 asym., 1313 sym, n C-Cl at 755. ^{13}C NMR (101 MHz, DMSO) δ 162.8 ppm (C=O), δ 153.0 ppm (N-(C=O)-N), δ 140.1 -111.8 ppm (CH aromatic) δ 101.6 ppm (N-C-N).

*2.2.4 7'-chloro-1-(4-hydroxyphenyl)-3-phenylspiro[[1,3]diazetidine-2,3'-indoline]-2',4-dione (**8**)*

Yield= 80%, light brown, m.p.= 220-222 FTIR (in KBr disk, 4000-400 cm^{-1}) ν O-H at 3326, ν N-H at 3290, aromatic νC-H at 3064, νC=O at 1723, ν N-C=O at 1649, ν C=C at 1618-1590, ν C-Cl at 781. ^{1}HNMR (400 MHz, DMSO-d6) δ 6.46– 7.28 ppm (m, C-H aromatic), δ 7.95 ppm (s, 1H, N-H), δ 8.64 ppm (s, 1H, O-H). ^{13}C NMR (101 MHz, DMSO) δ 162.2 ppm (C=O), δ 152.4 ppm (N-(C=O)-N), δ 139.6 -113.7 ppm (CH aromatic) δ 97.8 ppm (N-C-N).

*2.3 Synthesis of 7'-chloro-1-(4-aryl)-3-phenyl-4-thioxospiro[[1,3]diazetidine-2,3'-indolin]-2'-one (**9-12**)*[21]

A solution of phenyl isothiocyanate (3.58 mL, 30.0 mmol) and (30.0 mmol) Schiff bases derivatives (**1-4**) dissolved in 5 mL of DMF was reflexed for (20-23 hrs.). At the end, the reaction mixture cooled and was poured into ice water. The precipitated solid was filtered, washed with water and recrystallized from a suitable solvent.

*2.3.1 7'-chloro-1-(4-chlorophenyl)-3-phenyl-4-thioxospiro[[1,3]diazetidine-2,3'-indolin]-2'-one (**9**)*

Yield= 84%, Brown, m.p.=96-98 FTIR (in KBr disk, 4000-400 cm^{-1}) ν N-H at 3209, aromatic νC-H at 3035, νC=O at 1720, ν C=C at 1616-1595, ν N-C=S at 1232, ν C-Cl at 754. ^{13}C NMR (101 MHz, DMSO) δ 180.1 ppm (C=S), δ 165.4 ppm (C=O), δ 153.0-118.6 ppm (CH aromatic) δ 96.3 ppm (N-C-N).

*2.3.2 7'-chloro-1-(4-(dimethylamino)phenyl)-3-phenyl-4-thioxospiro[[1,3]diazetidine-2,3'-indolin]-2'-one (**10**)*

Yield= 87%, Black, m.p.=95-97 FTIR (in KBr disk, 4000-400 cm^{-1}) ν N-H at 3253, aromatic νC-H at 3053, ν -C-H at 2995, νC=O at 1721, ν C=C at 1620-1595, ν N-C=S at 1232, ν C-Cl at 754. ^{1}HNMR (400 MHz, DMSO-d6) δ 3.28 ppm (s, 6H, N-CH_3), δ 6.54 – 7.95 ppm (m, C-H aromatic), δ 8.65 ppm (, s, 1H, N-H). ^{13}C NMR (101 MHz, DMSO-d6) δ 179.5 ppm (C=S), δ 165.4 ppm (C=O), δ 152.4-112.7 ppm (CH aromatic) δ 99.5 ppm (N-C-N), δ 51.5 ppm ($N(CH_3)_2$).

*2.3.3 7'-chloro-1-(4-nitrophenyl)-3-phenyl-4-thioxospiro[[1,3]diazetidine-2,3'-indolin]-2'-one (**11**)*

Yield= 90%, Intense-yellow, m.p.= 104-106 FTIR (in KBr disk, 4000-400 cm^{-1}) ν N-H at 3292, aromatic νC-H at 3058, νC=O at 1723, ν C=C at 1618-1595, ν NO_2 at 1444 asym., 1313 sym., ν N-C=S at 1232, ν C-Cl at 752. ^{13}C NMR (101 MHz, DMSO) δ 179.3 ppm (C=S), δ 158.4 ppm (C=O), δ 152.2-113.3 ppm (CH aromatic) δ 90.5 ppm (N-C-N).

*2.3.4 7'-chloro-1-(4-hydroxyphenyl)-3-phenyl-4-thioxospiro[[1,3]diazetidine-2,3'-indolin]-2'-one (**12**)*

Yield= 84%, Brown, m.p.= 125-127 FTIR (in KBr disk, 4000-400 cm^{-1}) ν O-H at 3390, ν N-H at 3207, ν =C-H at 3035, νC=O at 1720, ν C=C at 1620-1594, ν N-C=S at 1234, ν C-Cl at 756. ^{13}C NMR (101 MHz, DMSO) δ 179.5 ppm (C=S), δ 165.4 ppm (C=O), δ 152.4-118.1 ppm (CH aromatic) δ 98.8 ppm (N-C-N).

2.4 In silico studies

2.4.1 ADME study

The Swiss ADME online server (http://www.swissadme.ch/) was used to determine the physicochemical parameters of each compound. The server calculates the physicochemical parameters of small molecules using an accurate and effective iLOG algorithm. The server provides a lot of important information about the pharmacokinetic profiles and drug-like nature [22].

2.4.2 Preparation of ligands

The compounds were initially represented as 2D structures using the software Chem Bio Draw 12.0. These 2D structures were then transformed into 3D models and saved in the .mol file format for further analysis. To optimize these structures, an energy minimization process was carried out for all ligands. This was done using the Avogadro 1.2 software, with the MMFF94S force field serving as the basis for the energy calculations. This process ensures that the 3D models of the compounds are in their lowest energy, and thus most stable, configurations.

2.4.3 Preparation of proteins for docking

All 3D structures of proteins (VEGFR-2 (PDB:4AGD)[23] and ALR2 (PDB code: 1Z3N)[15]) used for docking were retrieved from PDB and prepared using the Protein Preparation Wizard of Maestro 12.5. Preparation included hydrogen bond assignment, bond ordering, hydrogen addition, optimization, protein minimization, and deletion of water beyond 5 from the het group. The Glide-grid wizard was used to create a protein-receptor grid. The high potential binding site of the ligands was determined by selecting an atom of the protein co-crystallized ligand. The Van der Waals scaling factor was set to 1.0 and the partial charge cutoff was set to 0.25. In addition, docking of all ligands was performed using the ligand docking module of Glide. The system was configured to run in Extra-Precision (XP) mode, leaving all other parameters in the default settings. Then, the results were visualized and analyzed using BIOVIA Discovery Studio Visualizer in 2021. This software enabled detailed analysis of the data generated by the system.

2.5 In vitro study

2.5.1 Total antioxidant capacity[21]

The total antioxidant activity of the samples was determined by a slight modification of the established procedure for the synthesis of phosphomolybdenum complexes This enabled an accurate estimation of the antioxidant activity of the samples. A 100 mL aliquot of the sample was mixed with 500 mL of a reagent solution (0.6 M sulfuric acid, 28 mM sodium phosphate, and 4 mM ammonium molybdate) and incubated at 95 °C for 90 min at various concentrations (150, 100, 50, and 25 mg/mL). The mixture was then cooled to 25 °C and the absorbance of only 300 mL of the sample solution was determined using a microplate reader at a wavelength of 695 nm. Based on the optical density of the sample, the antioxidant activity was calculated. A high optical density value indicates that the sample has high antioxidant activity. Antioxidant capacity is expressed as the number of equivalents of ascorbic acid

2.5.2 Determination of the free radical scavenging activity by DPPH[24]

In microplate wells, 100 µL ethanolic solutions of different concentrations (150, 100, 50, 25 µg/mL) of each compound were mixed with 200 µL ethanolic solution of DPPH (0.1 M). The reaction mixture was then agitated for a duration of one minute. Following this, it was left to incubate at room temperature for a period of 30 minutes. This incubation period was necessary for the determination of the optical density (OD) of the mixture. This measure provides valuable information about the reaction's progress. The optical density was then measured at a wavelength of 517 nm using a microplate reader. Ascorbic acid was used as a positive control. The percent inhibition of the DPPH radical was calculated using the following formula.

$$DPPH\ inhibition\% = \frac{A^{\circ}-A}{A^{\circ}} \times 100\% \quad (1)$$

2.6 In Vivo study

2.6.1 Animals and Housing

This study has been conducted on thirty-two adult Wistar albino rats (aged 3 months and weighted 200±10gm). They were adapted after acclimatization (for two weeks) in the animal house of College of Veterinary Medicine, AL-Qadisiya University during the period extended from January, 2023 to march, 2023.They were housed in a well-ventilated rooms inside plastic cages (4 rats /cage) and feed on a standard pellet diet and supplemented with drinking water during the experiment. The room temperature was kept at 23±2ºC and 12-hour light/dark rhythm with light on from 06: 00 a.m. to 06: 00 p.m. along the experimented period.

2.6.2 Experiment Design:

Thirty-two (32) adult male rats were divided randomly and equally into four experimental groups (n=8) and handles as follows for eight weeks:

1. Control (C) group: Rats in this group were treated with intra peritoneal injection and oral intubation of normal saline.
2. D-fructose group (T1): Animals in this group were subjected to intra peritoneal injection of D-fructose in a dose (150 mg/kg/day)[25]
3. Compound **2** group (T2): The rats were intubated Compound 200 mg/0.5 mL DMSO/rat/ day.[26]
4. D-fructose and Compound 2 group (T3): Rats in this group were administered Compound 2 concurrently with intra peritoneal injection of 150 mg/kg.B.W. of D-fructose. Compound 2 was calculated as 0.2 mg dissolved in 1 mL DMSO.

2.6.3 Blood Samples Collection:

Blood samples were collected by cardiac puncture technical at the end of 2nd and 4th weeks of the experiment to be used later. The rats were put under general anesthesia by I.M injection of Ketamine (90 mg/kg B.W) and Xylazine (40 mg/kg B.W), blood samples had been collected directly from the heart of all rats by using a sterile syringe. Blood samples were kept in gel tubes. Serum was isolated from the coagulated blood samples by centrifugation at 3000 RPM for 15 min, then serum samples were dispensed into Eppendorf-tubes by using micropipette, stored in a freezer at -18 °C until they were used.

2.6.4 Determination of Serum Total Antioxidant Capacity concentration

Serum Total Antioxidant Capacity concentration was measured colorimetric ally using Total Antioxidant Capacity Assay Kit depending on Re *et al*.[27]

2.6.5 Determination of Serum Malondialdehyde (MDA) concentration

Serum MDA concentration was measured colorimetrically using trichloroacetic acid (TCA) and thiobarbituric (TBA). Serum MDA reaction with thiobarbituric acid forming a pink color compound of MDA_TBA2, intensity of this color could be measured by absorbance of light at 532 nm.[28]

2.6.6 Statistical Analysis

The acquired data were analyzed statistically by one-way ANOVA test utilizing the SPSS V.25 software. Least Significant Difference (LSD) test at the significance level of 0.05 was used to compare the trial groups' averages when there were significant differences between them.[29]

3. Results and discussion

Chloroisatin derivatives **1-12** are synthesized according to the following synthetic sequence in scheme 1.

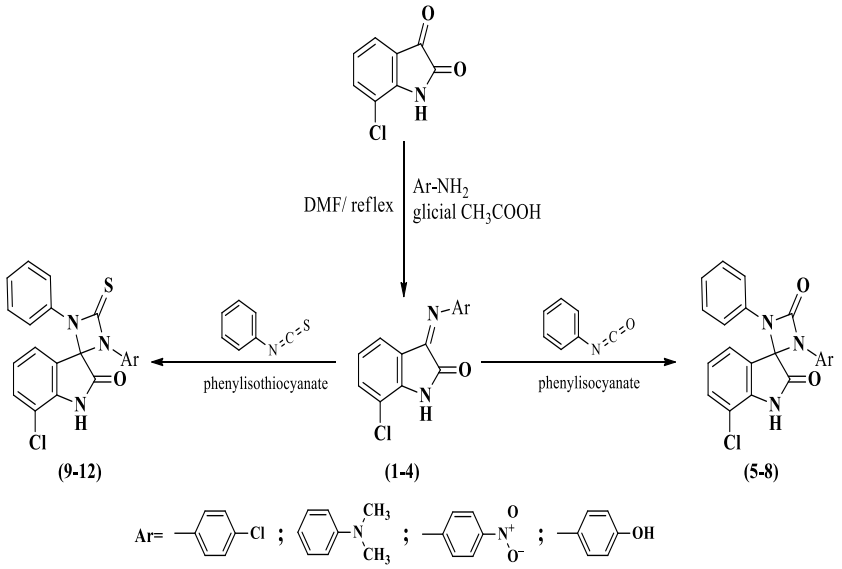

Scheme 1: Synthetic pathway of isatin derivatives **1-12**.

Schiff bases **1-4** are synthesized by rection of number of aromatic amines with 7-chloroisatin in DMF as solvent and glacial acetic acid as a catalyst. Synthesis of all compounds are characterized by ^{1}HNMR, ^{13}CNMR and FTIR spectra. FTIR spectra confirm synthesis of Schiff bases **1-4** by disappearance of stretching absorption band at (1749) cm^{-1} due to C=O groups and appearance of stretching absorption band at (1679-1670) cm^{-1} due to imine groups. In addition, the spectra showed some characteristic absorption bands due to the substituted groups on the benzene ring of the aromatic amines such as absorption band at (748-742) cm^{-1} due to C-Cl bond of compound **1**, absorption band at (2935) cm^{-1} due to aliphatic C-H bond of compound **2**, absorption band at (1475 asym, 1311 sym) cm^{-1} due to NO_2 group of compound **3** and absorption band at (3382) cm^{-1} due to O-H bond of compound **4**.

^{1}HNMR spectra confirm the formation of compounds **2-4** by appearance of their characteristic signals at (6.00 – 8.34) ppm due to CH aromatic protons and singlet signal at (8.12 - 8.75) ppm due to N-H proton. In addition, ^{1}HNMR spectra also shown singlet signal at (2.95) ppm due to aliphatic N-CH_3 proton of compound 2 and singlet signal at (8.93) ppm due to O-H proton of compound **4**.[30] The other characteristic signals of compounds **2-4** are mentioned previously in excremental section and showed in Figure 1.

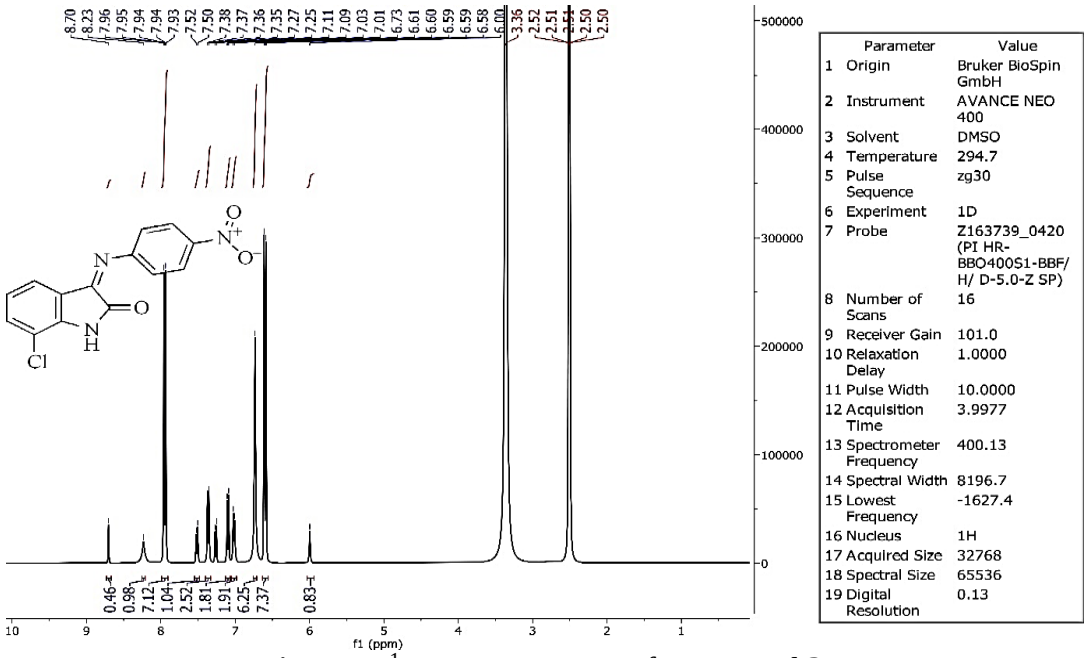

	Parameter	Value
1	Origin	Bruker BioSpin GmbH
2	Instrument	AVANCE NEO 400
3	Solvent	DMSO
4	Temperature	294.7
5	Pulse Sequence	zg30
6	Experiment	1D
7	Probe	Z163739_0420 (PI HR-BBO400S1-BBF/ H/ D-5.0-Z SP)
8	Number of Scans	16
9	Receiver Gain	101.0
10	Relaxation Delay	1.0000
11	Pulse Width	10.0000
12	Acquisition Time	3.9977
13	Spectrometer Frequency	400.13
14	Spectral Width	8196.7
15	Lowest Frequency	-1627.4
16	Nucleus	1H
17	Acquired Size	32768
18	Spectral Size	65536
19	Digital Resolution	0.13

Figure 1: ^{1}HNMR spectrum of compound **3**.

On other hand, ^{13}CNMR spectra confirm the formation of compound **3** mainly by appearance imine signals at (135.47) ppm. Also, ^{13}CNMR spectra show appearance of another characteristic signals such as signal at (155.61) ppm due to C=O group and signals at (128.88-104.56) ppm due to aromatic carbons. ^{13}CNMR spectrum of compound **3** showed in Figure 2.

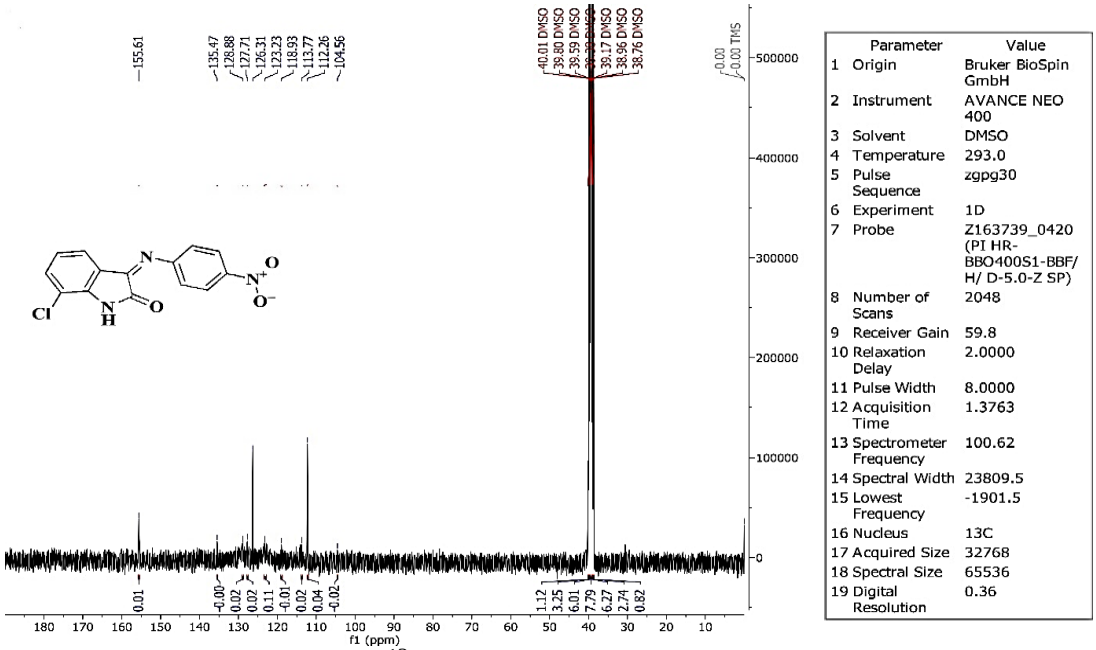

	Parameter	Value
1	Origin	Bruker BioSpin GmbH
2	Instrument	AVANCE NEO 400
3	Solvent	DMSO
4	Temperature	293.0
5	Pulse Sequence	zgpg30
6	Experiment	1D
7	Probe	Z163739_0420 (PI HR-BBO400S1-BBF/ H/ D-5.0-Z SP)
8	Number of Scans	2048
9	Receiver Gain	59.8
10	Relaxation Delay	2.0000
11	Pulse Width	8.0000
12	Acquisition Time	1.3763
13	Spectrometer Frequency	100.62
14	Spectral Width	23809.5
15	Lowest Frequency	-1901.5
16	Nucleus	13C
17	Acquired Size	32768
18	Spectral Size	65536
19	Digital Resolution	0.36

Figure 2:^{13}CNMR spectrum of compound **3**.

FTIR spectra confirm synthesis of compounds **5-8** by disappearance of stretching absorption band at (1679-1670) cm^{-1} due to imine groups and appearance of stretching absorption band at (1668-1633) cm^{-1} due to carbonyl group of diazetidine rings. In addition, the FTIR spectra showed stretching absorption band at (1726-1718) cm^{-1} due to C=O groups and stretching absorption band at (1621-1595) cm^{-1} due to C=C groups. Also, the FTIR spectra showed some characteristic absorption bands due to the substituted groups on the benzene ring of the

aromatic amines such as absorption band at (786) cm^{-1} due to C-Cl bond of compound **5**, absorption band at (2927) cm^{-1} due to aliphatic C-H bond of compound **6**, absorption band at (1444 asym., 1313 sym) cm^{-1} due to NO_2 group of compound **7** and absorption band at (3326) cm^{-1} due to O-H bond of compound **8**.[31]

^{1}HNMR spectra confirm the formation of compounds **6** and **8** by appearance of their characteristic signals at (6.46– 7.46) ppm due to CH aromatic protons and singlet signal at (7.95 - 8.67) ppm due to N-H proton. In addition, ^{1}HNMR spectra also shown singlet signal at (3.01) ppm due to aliphatic N-CH_3 proton of compound **6** and singlet signal at (8.64) ppm due to O-H proton of compound **8**. ^{1}HNMR spectrum of compound **6** showed in Figure 3.

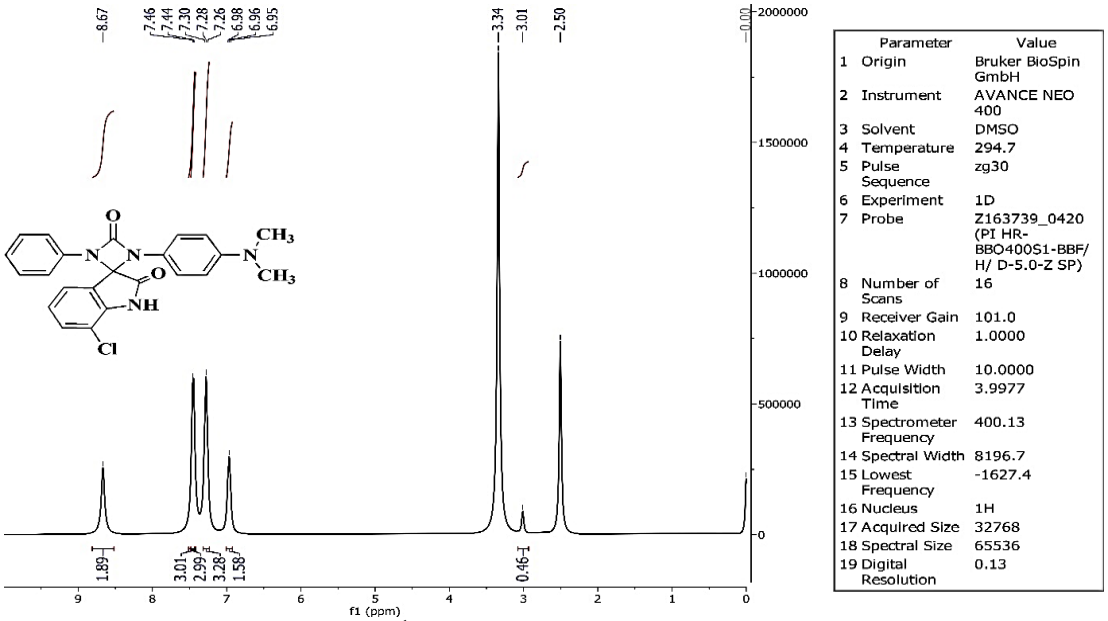

Figure 3: ^{1}HNMR spectrum of compound **6**.

On other hand, ^{13}CNMR spectra confirm the formation of compounds **5-8** mainly by appearance main signals such as carbonyl group of indole ring at (161.14-162.20) ppm, carbonyl group of diazetidine ring at (152.43-153.02) ppm and aromatic carbons CH at (106.10-140.19) ppm. Also, ^{13}CNMR spectra show appearance of signal at (51.38) ppm due to carbons of ($N(CH_3)_2$ group of compound **6**. ^{13}CNMR spectrum of compound **6** showed in Figure 4.

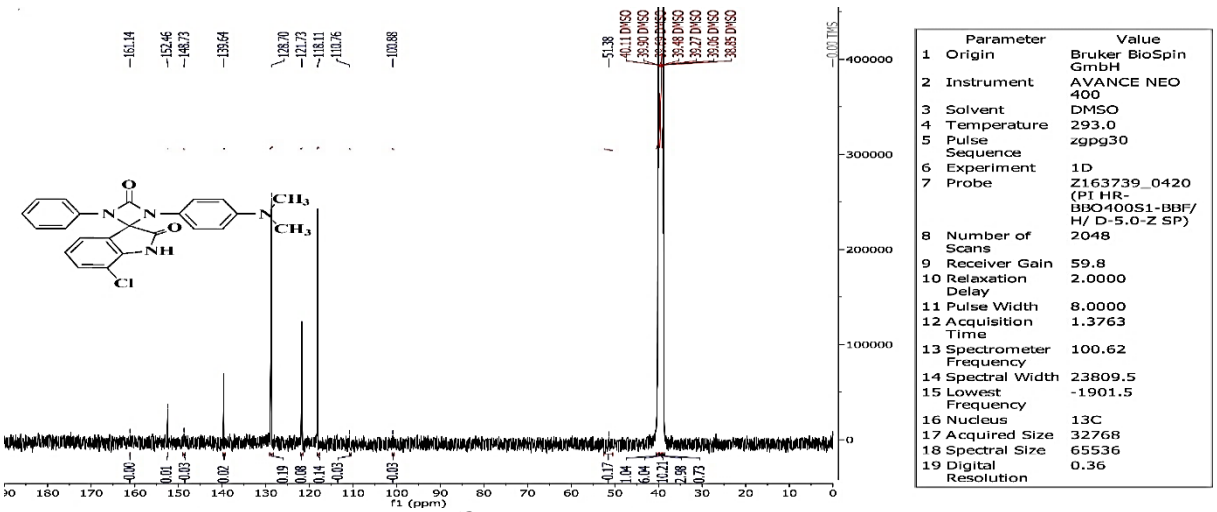

Figure 4: ^{13}CNMR spectrum of compound **6**

FTIR spectra confirm synthesis of compounds **9-12** by disappearance of stretching absorption band at (1679-1670) cm^{-1} due to imine groups and appearance of stretching absorption band at (1234-1232) cm^{-1} due to thiocarbonyl group of diazetidine rings. In addition, the FTIR spectra showed stretching absorption band at (1723-1720) cm^{-1} due to C=O groups and stretching absorption band at (1620-1594) cm^{-1} due to imine groups. Also, the FTIR spectra showed some characteristic absorption bands due to the substituted groups on the benzene ring of the aromatic amines such as absorption band at (754) cm^{-1} due to C-Cl bond of compound **9**, absorption band at (2995) cm^{-1} due to aliphatic C-H bond of compound **10**, absorption band at (1444 asym., 1313 sym) cm^{-1} due to NO_2 group of compound **11** and absorption band at (3390) cm^{-1} due to O-H bond of compound **12**.
^{1}HNMR spectra confirm the formation of compounds **10** by appearance of its characteristic signals such as singlet signal (3.28) ppm due to $N(CH_3)_2$ protons, multiple at (6.54 – 7.95) ppm due to CH aromatic protons and singlet signal at (8.65) ppm due to N-H proton. ^{1}HNMR spectrum of compound **10** showed in Figure 5.

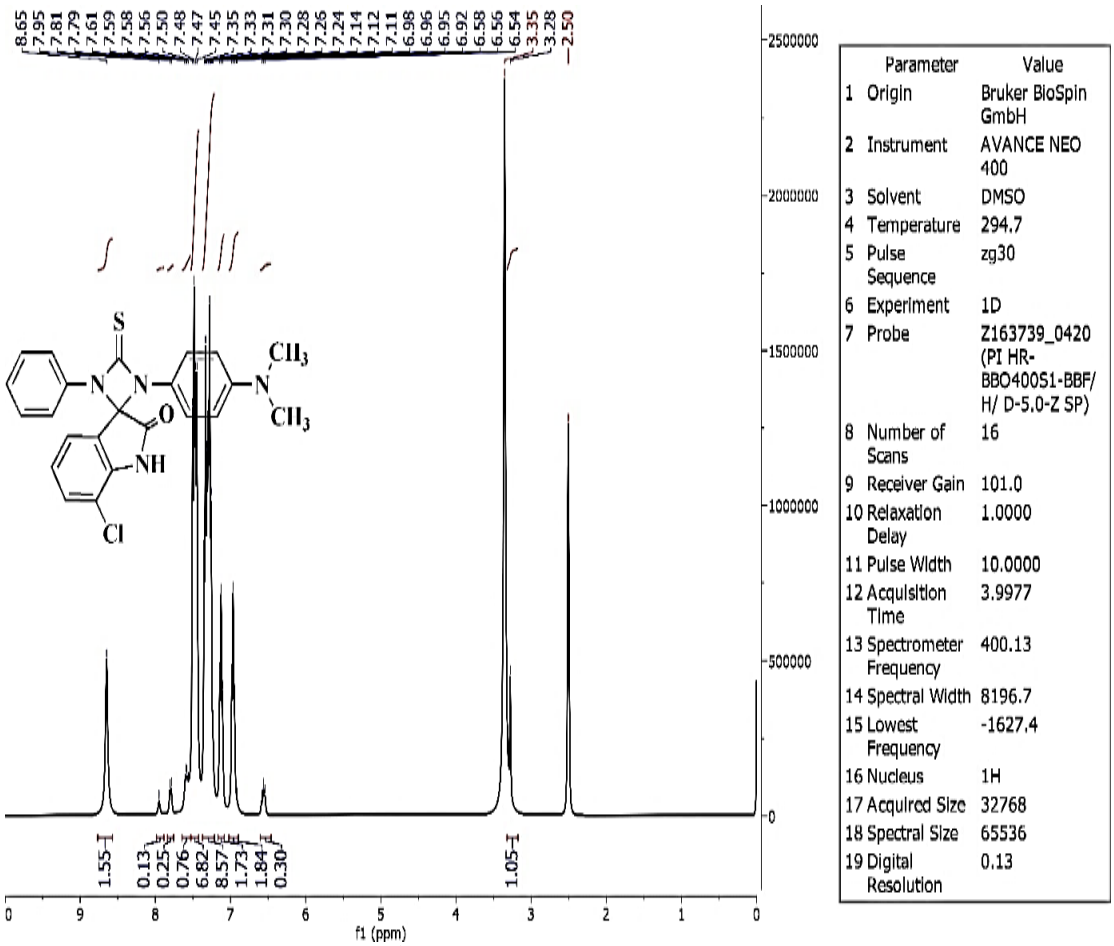

Figure 5: ^{1}HNMR spectrum of compound **10**.

On other hand, ^{13}CNMR spectra confirm the formation of compounds **9-12** mainly by appearance main signals such as thiocarbonyl group at (179.33 - 180.09) ppm, carbonyl group of indole ring at (165.46-158.44) ppm and aromatic carbons CH at (153.00-112.76) ppm. Also, ^{13}CNMR spectra show appearance of signal at (51.52) ppm due to carbons of $(N(CH_3)_2$ group of compound **10**. ^{13}CNMR spectrum of compound **10** showed in Figure 6.

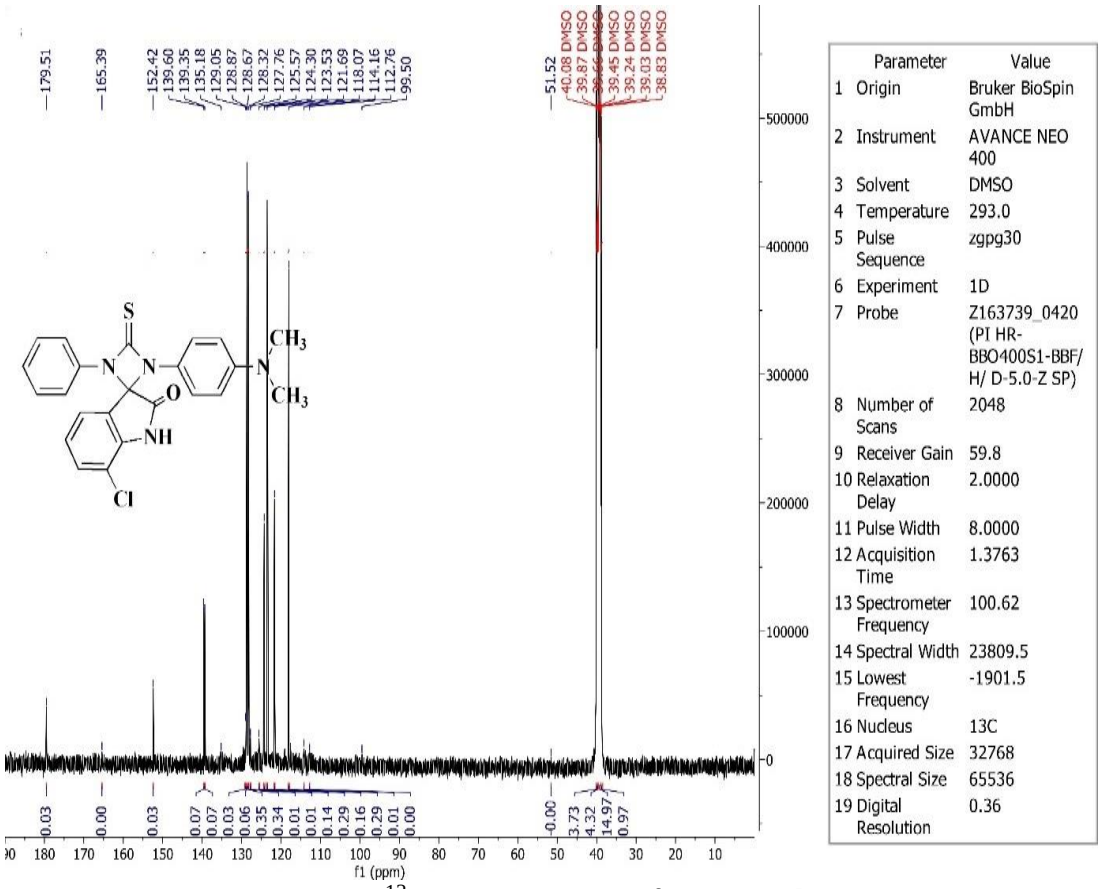

Figure 6: ^{13}CNMR spectrum of compound **10.**

3.1 In silico studies

3.1.1 ADME study

When a compound exhibits both the desired biological activity and an acceptable pharmacokinetic profile, it is seen as a potential candidate for drug discovery. Hence, in assessing their viability as drugs, both their pharmacodynamic and pharmacokinetic profiles are taken into account. The online tool SwissADME was used to calculate the ADME profiles and drug-like nature of all prepared compounds. This tool proved many useful parameters such as Physicochemical Properties, Lipophilicity, Water Solubility, Pharmacokinetics, Drug likeness and Medicinal Chemistry.

All the prepared compounds showed high bioavailability (bioavailability score = 0.55) due to their optimal physicochemical properties, as demonstrated in the bioavailability radar map. The map contains six critical parameters for oral absorption: polarity, saturation, lipophilicity, size, solubility and flexibility. The map control includes a pink area representing the acceptable ranges of the six parameters and red lines representing the calculated physicochemical properties of the compounds. All physicochemical properties of the prepared compounds were within the desired range for all parameters except saturation property as shown in Figure 7.

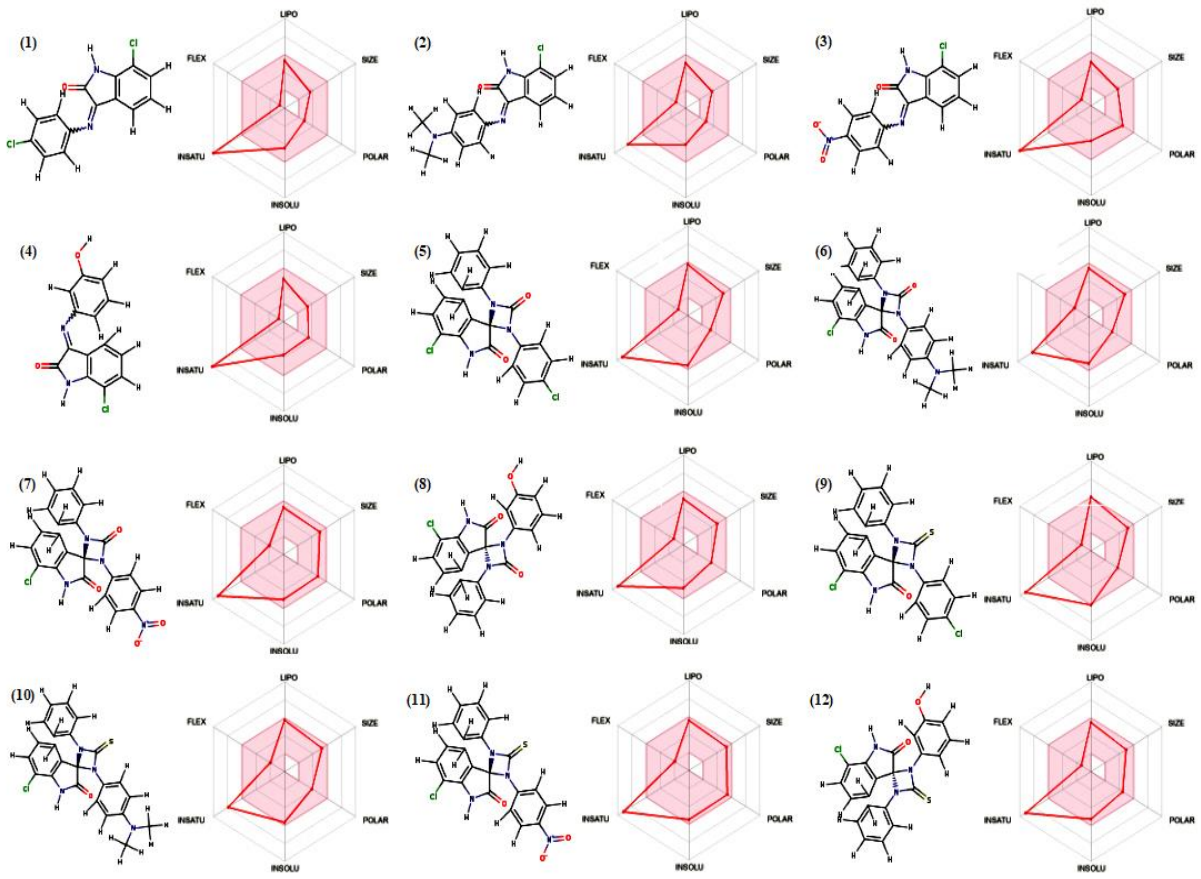

Figure 7: bioavailability radar map of compounds **1-12**

In dissuasion of Pharmacokinetics properties, all compounds shown high gastrointestinal absorption (GI) because they have acceptable topological polar surface areas (TPSA) that ranged between (41.46- 113.49) Å². Compounds **3**, **7**, **11**, and **12** may not penetrate the BBB and therefore can be used safely without CNS complications, whereas the other compounds may penetrate the BBB as shown in Table 1. Some of the prepared compounds **6**, **8**, **10** and **12** show their ability to act as substrates for the P-glycoprotein (P-gp). The P-gp is responsible for pumping drugs and toxins out of the cells into the lumen, which means that the bioavailability of these compounds within the cells might be reduced by this protein, while the other compounds do not act as substrates for this protein. The metabolism of all prepared compounds, as with most drugs, is determined in the liver by CYTP450 enzymes. Therefore, it is recommended to administer them alone to minimize possible drug-drug interactions.[32]

Table 1: Pharmacokinetics properties of compounds **1-12**.

No.	TPSA	GI absorption	BBB permeant	Pgp substrate	CYP1A2 inhibitor	CYP2C19 inhibitor	CYP2C9 inhibitor	CYP2D6 inhibitor	CYP3A4 inhibitor
1	41.46	High	Yes	No	Yes	Yes	Yes	No	Yes
2	44.7	High	Yes	No	Yes	Yes	Yes	Yes	Yes
3	87.28	High	No	No	Yes	Yes	Yes	No	Yes
4	61.69	High	Yes	No	Yes	No	No	Yes	Yes
5	52.65	High	Yes	No	Yes	Yes	Yes	No	No
6	55.89	High	Yes	Yes	No	Yes	Yes	Yes	Yes
7	98.47	High	No	No	No	Yes	Yes	No	No
8	72.88	High	Yes	Yes	Yes	Yes	Yes	Yes	No
9	67.67	High	Yes	No	Yes	Yes	Yes	No	Yes
10	70.91	High	Yes	Yes	No	Yes	Yes	Yes	Yes
11	113.49	High	No	No	No	Yes	Yes	No	Yes
12	87.9	High	No	Yes	Yes	Yes	Yes	No	Yes

In contrast, the majority of these compounds adhered to all the drug likeness guidelines as per Lipinski, Veber, and Muegge. However, a single alert was raised during the PAINS assay. This was attributed to the presence of aniline dialkyl functionality in compounds 2, 6, and 10, as detailed in Table 2 [33].

Table 2: drug likeness rules of compounds **1-12**

No	Lipinski	Veber	Muegge	Bioavailability Score	Leadlikeness violations	Synthetic Accessibility
1	0	0	0	0.55	1	2.55
2	0	0	0	0.55	0	2.83
3	0	0	0	0.55	0	2.69
4	0	0	0	0.55	0	2.55
5	1	0	0	0.55	2	3.68
6	0	0	0	0.55	2	3.95
7	0	0	0	0.55	2	3.81
8	0	0	0	0.55	1	3.76
9	1	0	1	0.55	2	3.82
10	0	0	0	0.55	2	4.09
11	0	0	0	0.55	2	3.94
12	0	0	0	0.55	2	3.88

3.1.2 Docking study of VEGFR-2

In this study, Maestro 11.5 was used to perform a docking study for all compounds **1-12** at the ATP-binding site of VEGFR-2 kinase. For the docking study, a high-resolution VEGFR-2 (PDB:4AGD) co-crystallized with sunitinib was used. Sunitinib was first docked to the active site of the VEGFR-2 enzyme to validate the docking procedure. With a docking score of -6.74 kcal/mol, sunitinib reproduced a binding pose similar to that of the co-crystallized ligand. Upon binding, sunitinib interacted with residues Glu917 and Cys919 of the hinge region by forming hydrogen bonds between NH and CO of the indolinone backbone and hydrogen bond between NH of amide and Leu810, in addition to hydrophobic contacts with the gatekeeper residues (Leu840 and Ala866), the hinge residues (Val916 and Phe918), Leu1035 Cys1045, Val899, Lys868, Phe1047 and Val848. Figure 8 represent the 2D and 3D interaction of VEGFR-2 with compound **1** and co-crystalized ligand sunitinib.

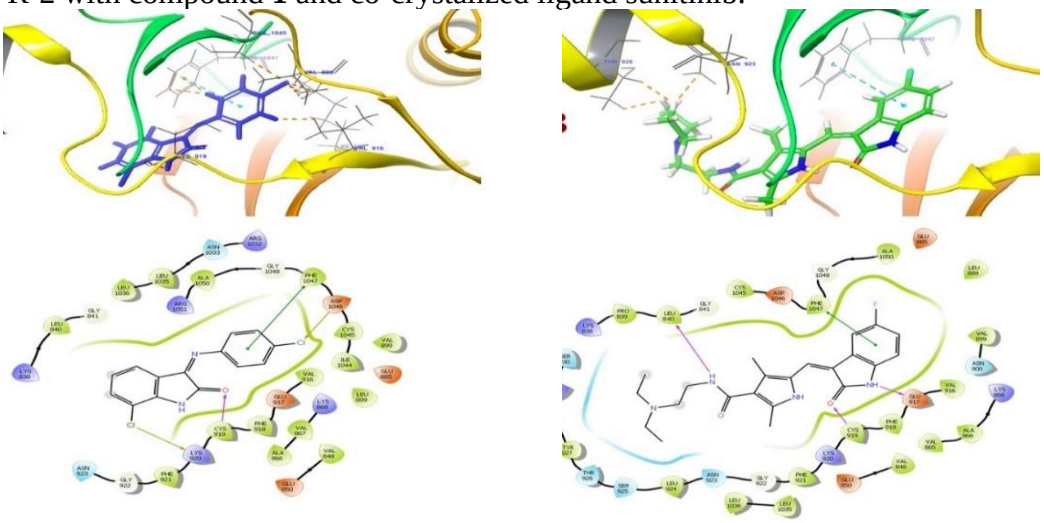

(a) **(b)**

Figure 8: 2D and 3D molecular interaction of VEGFR-2 with (a) compound **1**, (b) co-crystalized ligand sunitinib.

All compounds were docked to the ATP-binding site of VEGFR-2. It was found that the studied compounds 1-4 were well fitted into the ATP-binding site of VEGFR-2 with binding energies of 6.60, 6.70, 4.99, and 5.01 kcal/mol, respectively, whereas the other compounds **5-12** had moderate to weak binding energies in the range of (5-2 kcal/mol). This is due to the linear structures of **1-4** resembling those of sunitinib, while the structures of the other compounds **5-12** are large and sterically hindered, causing them to be displaced from the binding site. In addition, the docked compounds **1-4** showed a convergent binding pattern similar to that of sunitinib, in which hydrogen bonds were observed between the NH and CO of the indolinone backbone and the key residues Cys919 and Glu917 in the hinge region. Additionally, the isatin moiety in compounds **1-4** was fitted into a hydrophobic pocket lined with residues Leu840, Val848, and Phe1047. This hydrophobic interaction could likely enhance the binding affinity of the inhibitors to the active site of VEGFR-2. Moreover, the benzene rings and their para substituents of compounds **1-4** play an important role in binding to the active site by forming specific interactions that largely affect the binding energy and orientation of the ligand, such as hydrophobic interactions of substituents -Cl and -$N(CH_3)_2$ or hydrogen bonding of substituent - OH.

Table 3: Docking results of compounds **1-12** with VEGFR-2protein.

No.	docking score	XP GScore	glide gscore	glide rmsd	Hb interactions	Hydrophobic interactions
1	-8.529	-8.529	-8.529	49.79	Cys919	Leu840, Ala866, Val916, Phe918, Leu1035, Cys1045, Val899, Lys868, Phe1047, Val848
2	-5.237	-5.237	-5.237	52.552	Glu917, Cys919	Leu840, Ala866, Val916, Phe918, Leu1035, Val899, Lys868, Val848
3	-5.424	-5.424	-5.424	51.36	-	Leu840, Ala866, Val916, Leu1035, Lys868, Val848, Cys919
4	-6.274	-6.274	-6.274	51.848	Leu840	Leu840, Ala866, Leu1035, Cys1045, Phe1047, Val848, Cys919
5	-3.872	-3.872	-3.872	55.592	Asn923	Leu840, Phe918, Cys919, Gly922
6	-3.973	-3.973	-3.973	55.316	Leu840	Ala866, Leu1035, Phe1047, Val848
7	-3.288	-3.288	-3.288	55.173	Cys919, Asn923	Leu840, Gly922
8	-4.637	-4.637	-4.637	55.768	Asn923, Lys920	Leu840
9	-3.07	-3.07	-3.07	56.004	Cys919, Asn923, Lys920	Leu840, Val848
10	-3.296	-3.296	-3.296	57.214	Lys838	Cys919, Leu1035, Phe1047, Leu840
11	-3.453	-3.453	-3.453	56.087	Asn923, Lys920	Leu840, Val848, Phe921
12	-2.317	-2.317	-2.317	56.432	Lys920, Lys838	Leu840
st	-11.868	-11.868	-11.868	52.667	Glu917, Cys919, Leu810	Leu840, Ala866, Val916, Phe918, Leu1035, Cys1045, Val899, Lys868, Phe1047, Val848

3.1.3 Docking study of ALR2

The lidorestat-bound ALR2 (PDB code: 1Z3N) was chosen for the docking study owing to the structural similarity of the synthetic compound and the ligand. As we do with Sunitinib, lidorestat was first docked to the active site of the ALR2 enzyme to validate the docking procedure. With a docking score of -14.461, lidorestat reproduced a binding pose similar to that of the co-crystallized ligand. lidorestat form hydrogen bonding with (Tyr48, Cys80, Hie110, Trp111, Leu300) residues and hydrophobic interactions with (Trp20, Trp79, Trp111, Phe122, Cys298, Ala299, Cys303, Pro310) residues of binding pocket. Figure 9. Represents 2D and 3D molecular interaction of ALR2 with (a) compound 1, (b) co-crystalized ligand lidorestat

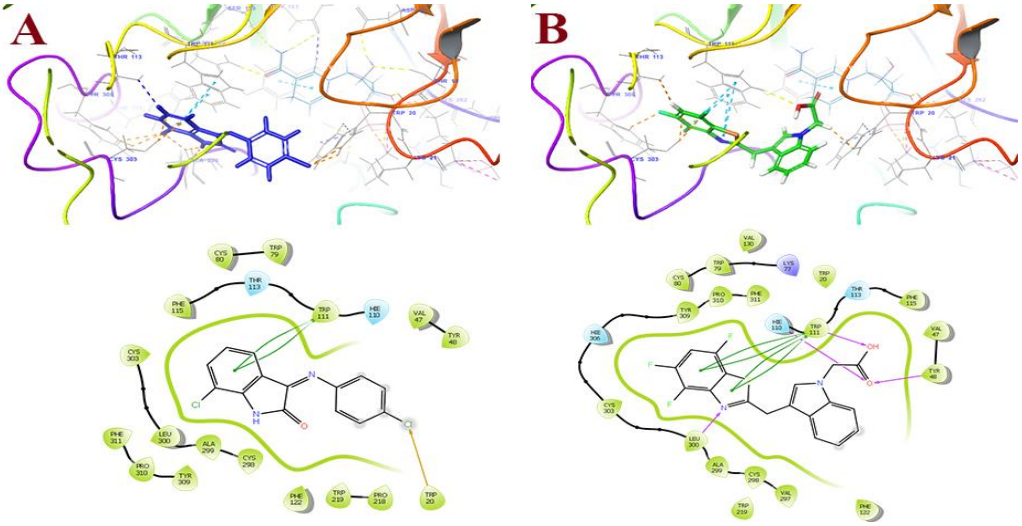

(a) **(b)**

Figure 10: 2D and 3D molecular interaction of ALR2 with (a) compound **1**, (b) co-crystalized ligand lidorestat

All compounds were docked to the active binding site of ALR2. As it happened in the docking with an enzyme. It was found that the studied compounds 1-4 were well fitted into the binding site of the ALR2 enzyme with docking score ranged between -8.895 to -8.594, whereas the other compounds **5-12** also had moderate to weak docking score ranged between (-7.845 - -5.329). This is due to the structural similarities between compounds **1-4** and co-crystallized ligand, while the bulk structures of compounds **5-12** also hindered it from making strong interactions with the active site of the enzyme and displaced it outside. Compounds **1-4** showed a high dependence on hydrophobic interactions with the residues of the active site and almost similar to that of lidorestat. While we note the lack of building hydrogen bonds with these compounds compared to lidorestat due to the low number of heterogeneous atoms in it. Moreover, the benzene rings and their para substituents of compounds **1-4** play an important role in binding to the active site by forming specific interactions that largely affect the binding energy and orientation of the ligand, such as hydrophobic interactions of substituents -Cl and $-N(CH_3)_2$ or hydrogen bonding of substituent - OH.

Table 4: Docking results of compounds **1-12** with ALR2 protein.

No.	docking score	XP GScore	glide gscore	glide rmsd	Hb interactions	Hydrophobic interactions
1	-8.895	-8.895	-8.895	23.711	-	TRP20, TRP111, ALA299, LEU300, CYS303, PHE311
2	-8.594	-8.594	-8.594	24.449	-	TRP20, VAL47, TRP111, PRO218, PHE122, LEU300, CYS303, TYR309, PHE311
3	-8.724	-8.724	-8.724	23.595	TRP20	TRP111, PHE122, LEU300, CYS303, TYR309, PRO310, PHE311
4	-8.82	-8.82	-8.82	23.701	TRP20	TRP111, ALA299, LEU300, CYS303, TYR309, PHE311
5	-6.363	-6.363	-6.363	27.065	VAL47	TYR48, NDP318, TRP20, TRP79, HIE110, TRP111, LYS21
6	-5.874	-5.874	-5.874	26.134	TRP20	TRP111, PHE122, LEU300, TRP219
7	-5.329	-5.329	-5.329	27.309	TRP20	PHE122
8	-7.845	-7.845	-7.845	26.609	VAL47	TRP20, PHE122, PRO218
9	-7.168	-7.168	-7.168	27.092		TYR48, TRP20, NDP318, HIE110, TRP111
10	-6.385	-6.385	-6.385	26.838		VAL47, PRO218
11	-6.139	-6.139	-6.139	27.35	VAL47, TRP48, HIE110	TRP20, VAL47
12	-6.474	-6.474	-6.474	27.179	VAL47	TRP20, VAL47, TYR48
st	-14.461	-14.461	-14.461	23.731	TYR48, CYS80, HIE110, TRP111, LEU300	TRP20, TRP79, TRP111, PHE122, CYS298, ALA299, CYS303, PRO310

3.2 In Vitro Study

3.2.1 Total antioxidant capacity

The synthesized compounds **1-12** were assessed for their total antioxidant capacity using the phosphomolybdenum method. This method is based on the conversion of Molybdenum (VI) to Molybdenum(V) via reduction by the synthesized compounds, resulting in the formation of a green phosphate – Mo (V) complex in acidic pH. Ascorbic acid was used as a standard to compare the antioxidant activity of the compounds. Table 5. and Figure 10. show that the isatin derivatives **1-12** exhibited good to moderate antioxidant capacity against reduced Mo (VI). The antioxidant capacity of the synthesized compounds was found to be influenced by the nature and position of substituent groups on the benzene ring. Compounds possess hydroxyl and amine groups exhibited significantly greater antioxidant capacity than those without such groups. Specifically, compounds **2**, **3**, **7**, **8** and **12** displayed remarkably high antioxidant activity compared to the standard, indicating their potential use as effective antioxidants.

Table 5: Total antioxidant capacity of compounds .**1-12**.

No.	Total antioxidant capacity			
	100 (mg/ml)	200 (mg/ml)	300 (mg/ml)	400 (mg/ml)
1	0.508	0.676	0.812	0.912
2	0.605	0.804	0.949	1.073
3	0.528	0.689	0.925	1.103
4	0.486	0.615	0.747	0.839
5	0.479	0.642	0.789	0.935
6	0.487	0.593	0.786	0.98
7	0.519	0.686	0.852	1.033
8	0.517	0.757	0.996	1.163
9	0.516	0.679	0.77	0.976
10	0.362	0.479	0.593	0.73
11	0.461	0.619	0.766	0.875
12	0.71	0.916	1.1	1.299
st	0.132	0.343	0.553	0.744

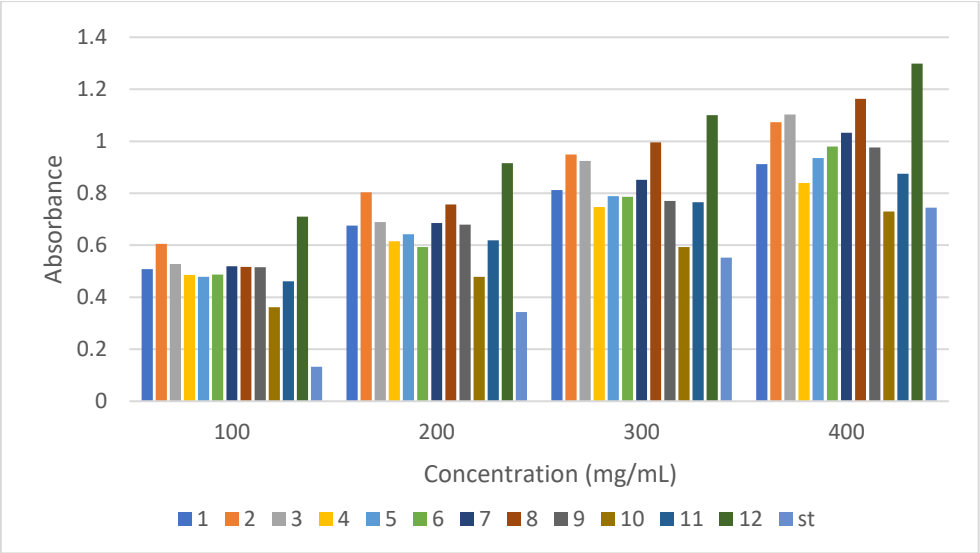

Figure 10: Total antioxidant capacity of compounds **1-12**.

3.2.2 Free radical scavenging activity

The Free Radical Scavenging Activity (FRSA) test, a widely utilized assay, gauges the antioxidant potential of natural substances, synthetic compounds, or plant-derived extracts. This test operates on the understanding that antioxidants can counteract free radicals through the donation of electrons or hydrogen atoms, thus averting oxidative harm to cells and tissues. The FRSA test involves the use of a stable free radical compound, such as 2,2-diphenyl-1-picrylhydrazyl (DPPH), which is purple in color. When DPPH reacts with an antioxidant, the purple color disappears due to the transfer of hydrogen atoms from the antioxidant to the DPPH radical, resulting in the formation of a yellow-colored product. The degree of discoloration is measured spectrophotometrically and is directly proportional to the scavenging activity of the antioxidant.[34]

All the synthesized compounds **1-12** were assessed for their free radical scavenging activity. According to the results presented in Table 10 and Figure 11, the synthesized compounds demonstrated favorable to moderate activity in comparison to the standard. Notably, compounds **3**, **4**, **10**, and **12** exhibited particularly potent efficacy, potentially attributed to the influence of the substituent groups on the benzene ring and the degrees of solubility.

Table 6: Free radical scavenging activity of compounds **1-12**.

No.	Free radical scavenging activity			
	100 (mg/ml)	200 (mg/ml)	300 (mg/ml)	400 (mg/ml)
1	35.36%	44.07%	52.64%	56.71%
2	23.21%	34.93%	36.57%	41.79%
3	49.79%	62.43%	66.93%	70.50%
4	63.00%	68.43%	71.14%	74.64%
5	24.71%	25.36%	25.64%	28.07%
6	26.57%	33.86%	36.57%	37.71%
7	25.00%	28.00%	32.64%	32.86%
8	4.57%	10.79%	15.57%	18.07%
9	36.00%	43.36%	47.93%	53.29%
10	58.79%	63.00%	64.86%	68.36%
11	41.86%	48.50%	53.21%	59.29%
12	48.07%	52.57%	54.71%	59.64%
St	27.68%	42.37%	55.65%	65.82%

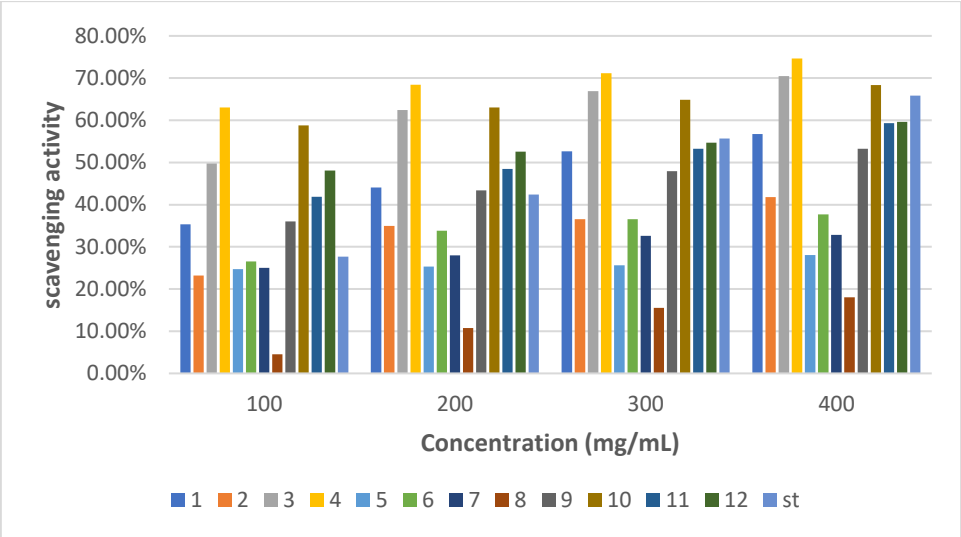

Figure 11: free radical scavenging activity by DPPH of compounds **1-12**

3.3 In vivo study

In order to validate the findings derived from *in silico* and *in vitro* investigations regarding the potential antioxidative activities of the prepared compounds, Compound **2** was selected as the subject of inquiry to assess its *in vivo* antioxidant activity. The assessment was conducted on an animal model. The experimental design involved the division of rats into three distinct groups, along with a control group as mentioned previously. The first group (T1) was subjected to oxidative stress through L-D-fructose administration to induce a heightened oxidative state within the animals. The second group (T2) was administered a specific dosage of Compound **2** (200 mg/0.5ml DMSO/rat/ day) to investigate its isolated effect on the animal's physiological system. Lastly, the third group (T3) was administered a mixture containing Compound **2** and D-fructose to evaluate the potential antioxidative abilities of the compound under study. The evaluation was performed by measuring the concentration of Total antioxidant capacity and Malondialdehyde (MDA) levels in the serum of the rats' groups.

3.3.1 Total antioxidant capacity (TAO-C) concentration in serum male rats:

Serum total antioxidant capacity concentration in all treated groups were clarified in Table 7. The results shown significant decrease ($p < 0.05$) in serum TAC in group (T1) at the 2nd and 4th weeks of experiment while the TAC in groups (T2 and T3) It remained almost constant compared to the control group at the end of experiment. which refers to positive and effective role of Compound **2** in preventing oxidative stress induced by D-fructose. Table 7. Represent Total antioxidant capacity (TAO-C) concentration (U/mL) in serum male rats.

Table 7: Total antioxidant capacity (TAO-C) concentration (U/mL) in serum male rats

After 15 days			After 30 days		
Group	**Mean ± SE**	**Absolute difference**	**Group**	**Mean ± SE**	**Absolute difference**
Control	4.43 ± 0.301	LSD = 0.392	*Control*	4.43 ± 0.301	LSD = 0.521
T1	2.14 ± 0.141	2.29 (significant)	*T1*	2.76 ± 0.434	1.67 (significant)
T2	4.41 ± 0.251	0.025 (no significant)	*T2*	4.65 ± 0.258	0.2225 (no significant)
T3	3.59 ± 0.290	0.84 (significant)	*T3*	4.20 ± 0.333	0.23 (no significant)

3.3.2 Malondialdehyde (MDA) concentration in serum male rats:

Malondialdehyde is a measure of lipid peroxidation in the tissues, which considered as one of the important markers of oxidative stress that affect different organs.[35] Malondialdehyde (MDA) concentration in all treated groups were clarified in Table 8. The results shown significant increase ($p < 0.05$) in serum MDA in group (T1) at the 4th weeks of experiment which mean increasing the damage caused by oxidative stress induced by D-Fructose. In groups (T3), the MDA concentration remained almost constant compared to the control group at the end of experiment. This means that compound **2** effectively reduced the damage caused by oxidative stress induced by D-fructose. Within group (T2), compound 2 demonstrated no notable alteration in the concentration of Malondialdehyde (MDA), indicating it did not exert any detrimental impact on the animal's physiology. Refer to Table 8 for the representation of MDA concentration in the serum of male rats.

Table 8: Malondialdehyde (MDA) concentration (µmol/L) in serum male rats

After 15 days			After 30 days		
Group	**Mean ± SE**	**Absolute difference**	**Group**	**Mean ± SE**	**Absolute difference**
Control	0.15 ± 0.004	LSD = 0.014	*Control*	0.15 ± 0.004	LSD = 0.018
T1	0.14 ± 0.002	0.0125 (significant)	*T1*	0.19 ± 0.010	0.0325 (significant)
T2	0.09 ± 0.017	0.0625 (no significant)	*T2*	0.15 ± 0.019	0.0075 (no significant)
T3	0.11 ± 0.006	0.04 (no significant)	*T3*	0.14 ± 0.007	0.015 (no significant)

4. Conclusion

In the terms of bioactive compound synthesis, a novel series of azetidine and thioazetidine molecules, which incorporate an isatin component, have been effectively synthesized. This was achieved by instigating a reaction between the Schiff base derivatives of 7-chloroisatin and two compounds: phenylisocyanate and phenylthioisocyanate. The successful synthesis of these molecules marks a significant advancement in the field. The investigation of their bioactivity as antioxidants through *in silico*, *in vitro*, and *in vivo* studies revealed promising results. *In silico* analysis conducted showed that all compounds possessed favorable pharmacokinetic and pharmacodynamic properties. Molecular docking studies with VEGFR-2 and ALR2 proteins indicated that compounds **1-4** exhibited good docking scores. *In vitro* assessments using the total antioxidant capacity method and the DPPH power scavenging method demonstrated that all compounds displayed noteworthy to excellent antioxidant activity. However, compounds **2**, **3**, **7**, **8** and **12** stood out as a particularly potent antioxidant. For further evaluation, compound **2** was selected for an *in vivo* study involving male rats. The results confirmed its commendable performance as an effective antioxidant agent. Overall, the newly synthesized compounds, particularly compound **2**, can play as promising candidates for further development as antioxidants, with implications for potential therapeutic applications in combating oxidative stress-related diseases. Further investigations and optimization of these molecules may offer valuable insights into the development of novel antioxidant-based treatments.

5. Disclosure and conflict of interest

The authors declare that they have no conflicts of interest.

References

[1] G. Pizzino, N. Irrera, M. Cucinotta, G. Pallio, F. Mannino, V. Arcoraci, F. Squadrito, D. Altavilla, and A. Bitto, "Oxidative Stress: Harms and Benefits for Human Health", *Oxid Med Cell Longev*, vol. 2017, p. 8416763,2017.

[2] H. Sato, M. Shibata, T. Shimizu, S. Shibata, H. Toriumi, T. Ebine, T. Kuroi, T. Iwashita, M. Funakubo, Y. Kayama, C. Akazawa, K. Wajima, T. Nakagawa, H. Okano, and N. Suzuki, "Differential cellular localization of antioxidant enzymes in the trigeminal ganglion", *Neuroscience*, vol. 248, pp. 345-58,2013.

[3] P. Rajendran, N. Nandakumar, T. Rengarajan, R. Palaniswami, E. N. Gnanadhas, U. Lakshminarasaiah, J. Gopas, and I. Nishigaki, "Antioxidants and human diseases", *Clinica Chimica Acta,* vol. 436, pp. 332-347,2014.

[4] L. A. Pham-Huy, H. He, and C. Pham-Huy, "Free radicals, antioxidants in disease and health", *International journal of biomedical science,* vol. 4, no. 2, pp. 89-96,2008.

[5] Y. Taniyama and K. K. Griendling, "Reactive Oxygen Species in the Vasculature", *molecular and cellular mechanisms*, vol. 42, no. 6, pp. 1075-1081,2003.

[6] F. Sonmez, Z. Gunesli, B. Z. Kurt, I. Gazioglu, D. Avci, and M. Kucukislamoglu, "Synthesis, antioxidant activity and SAR study of novel spiro-isatin-based Schiff bases", *Molecular Diversity,* vol. 23, no. 4, pp. 829-844,2019.

[7] T. B. S. Giorno, B. V. d. Silva, A. d. C. Pinto, and P. D. Fernandes, "Antinociceptive effect and mechanism of action of isatin, N-methyl isatin and oxopropyl isatin in mice", *Life Sciences*, vol. 151, pp. 189-198,2016.

[8] T. E. Malah, H. Farag, B. A. Hemdan, R. E. Abdel Mageid, M. T. Abdelrahman, M. A. El-Manawaty, and H. F. Nour, "Synthesis, in vitro antimicrobial evaluation, and molecular docking studies of new isatin-1,2,3-triazole hybrids", *Journal of Molecular Structure,* vol. 1250, p. 131855,2022.

[9] T. Kundu and A. Pramanik, "Convenient synthesis and evaluation of antioxidant property of functionalized spiro indolinone-dihydroquinazolinones", *Bioorganic Chemistry,* vol. 124, p. 105830,2022.

[10] M. Eldeeb, E. F. Sanad, A. Ragab, Y. A. Ammar, K. Mahmoud, M. M. Ali, and N. M. Hamdy, "Anticancer Effects with Molecular Docking Confirmation of Newly Synthesized Isatin Sulfonamide Molecular Hybrid Derivatives against Hepatic Cancer Cell Lines", vol. 10, no. 3, pp. 722-743,2022.

[11] S. Mehreen, M. Zia, A. Khan, J. Hussain, S. Ullah, M. U. Anwar, A. Al-Harrasi, and M. M. Naseer, "Phenoxy pendant isatins as potent α-glucosidase inhibitors: reciprocal carbonyl···carbonyl interactions, antiparallel π···π stacking driven solid state self-assembly and biological evaluation", *RSC Advances,* vol. 12, no. 32, pp. 20919-20928,2022.

[12] H. Singh, J. V. Singh, M. K. Gupta, A. K. Saxena, S. Sharma, K. Nepali, and P. M. S. Bedi, "Triazole tethered isatin-coumarin based molecular hybrids as novel antitubulin agents: Design, synthesis, biological investigation and docking studies", *Bioorganic & Medicinal Chemistry Letters*, vol. 27, no. 17, pp. 3974-3979,2017.

[13] D. Visagaperumal, J. E. Ezekwem, H. Munji, and V. Chandy, "Isatin schiff base-an overview", *PharmaTutor,* vol. 6, no. 5, pp. 38-47,2018.

[14] R. E. Ferraz de Paiva, E. G. Vieira, D. Rodrigues da Silva, C. A. Wegermann, and A. M. Costa Ferreira, "Anticancer Compounds Based on Isatin-Derivatives: Strategies to Ameliorate Selectivity and Efficiency", *Frontiers in Molecular Biosciences,* vol. 7, p. 627272,2021.

[15] M. C. Van Zandt, M. L. Jones, D. E. Gunn, L. S. Geraci, J. H. Jones, D. R. Sawicki, J. Sredy, J. L. Jacot, A. T. DiCioccio, T. Petrova, A. Mitschler, and A. D. Podjarny, "Discovery of 3-[(4,5,7-Trifluorobenzothiazol-2-yl)methyl]indole-N-acetic Acid (Lidorestat) and Congeners as Highly Potent and Selective Inhibitors of Aldose Reductase for Treatment of Chronic Diabetic Complications", *Journal of Medicinal Chemistry,* vol. 48, no. 9, pp. 3141-3152,2005.

[16] X. Hao, Z. Han, Y. Li, C. Li, X. Wang, X. Zhang, Q. Yang, B. Ma, and C. Zhu, "Synthesis and structure–activity relationship studies of phenolic hydroxyl derivatives based on quinoxalinone as aldose reductase inhibitors with antioxidant activity", *Bioorganic & Medicinal Chemistry Letters,* vol. 27, no. 4, pp. 887-892,2017.

[17] D. Sergi, J. Renaud, N. Simola, and M.-G. Martinoli, "Diabetes, a Contemporary Risk for Parkinson's Disease: Epidemiological and Cellular Evidences", *Frontiers in Aging Neuroscience,* vol. 11, p. 302,2019.

[18] L.-j. Yan, "Redox imbalance stress in diabetes mellitus: Role of the polyol pathway", *Animal Models and Experimental Medicine,* vol. 1, no. 1, pp. 7-13,2018.

[19] Y. Ji, X. Chen, H. Chen, X. Zhang, Z. Fan, L. Xie, B. Ma, and C. Zhu, "Designing of acyl sulphonamide based quinoxalinones as multifunctional aldose reductase inhibitors", *Bioorganic & Medicinal Chemistry,* vol. 27, no. 8, pp. 1658-1669,2019.

[20] M. G. Al-Khuzaie and S. M. Al-Majidi, "Synthesis and Characterization of Some New Benzothiazine, Dihydroquinazolinone and Oxazepine Derivatives from 1, 8-Naphthalic Anhydride and Evaluation of Their Antimicrobial Activity", *Journal of Global Pharma Technology*, vol. 10(11 (Suppl.)), pp. 415-423,2018.

[21] H. J. Al-Adhami, S. M. Al-Majidi, T. H. Mathkor, and Technology, "Synthesis and Identification of some new β-Lactam derivatives from 6-amino-1, 3-dimethyluracil and study their antioxidant activity", *Research Journal of Pharmacy and Technology*, vol. 13, no. 11, pp. 5317-5327,2020.

[22] A. Daina, O. Michielin, and V. Zoete, "SwissADME: a free web tool to evaluate pharmacokinetics, drug-likeness and medicinal chemistry friendliness of small molecules", *Scientific Reports*, vol. 7, no. 1, p. 42717,2017.

[23] M. McTigue, B. W. Murray, J. H. Chen, Y.-L. Deng, J. Solowiej, and R. S. Kania, "Molecular conformations, interactions, and properties associated with drug efficiency and clinical performance among VEGFR TK inhibitors", *Proceedings of the National Academy of Sciences of the United States of America*, vol. 109, no. 45, pp. 18281-18289,2012.

[24] R. S. Nayab, S. Maddila, M. P. Krishna, S. J. J. Titinchi, B. S. Thaslim, V. Chintha, R. Wudayagiri, V. Nagam, V. Tartte, S. Chinnam, and N. R. Chamarthi, "In silico molecular docking and in vitro antioxidant activity studies of novel α-aminophosphonates bearing 6-amino-1,3-dimethyl uracil", *Journal of Receptors and Signal Transduction*, vol. 40, no. 2, pp. 166-172,2020.

[25] Y.-M. Chang, H.-H. Chang, H.-J. Lin, C.-C. Tsai, C.-T. Tsai, H.-N. Chang, S.-L. Lin, V. PadmaViswanadha, R.-J. Chen, and C.-Y. Huang, "Inhibition of Cardiac Hypertrophy Effects in D-Galactose-Induced Senescent Hearts by Alpinate Oxyphyllae Fructus Treatment", *Evidence-Based Complementary and Alternative Medicine*, vol. 2017, p. 2624384,2017.

[26] N. D. Thanh, N. T. K. Giang, T. H. Quyen, D. T. Huong, and V. N. Toan, "Synthesis and evaluation of in vivo antioxidant, in vitro antibacterial, MRSA and antifungal activity of novel substituted isatin N-(2,3,4,6-tetra-O-acetyl-β-d-glucopyranosyl)thiosemicarbazones", *European Journal of Medicinal Chemistry*, vol. 123, pp. 532-543,2016.

[27] R. Re, N. Pellegrini, A. Proteggente, A. Pannala, M. Yang, and C. Rice-Evans, "Antioxidant activity applying an improved ABTS radical cation decolorization assay", *Free Radical Biology and Medicine*, vol. 26, no. 9, pp. 1231-1237,1999.

[28] N. A. M. Ghonimi, K. A. Elsharkawi, D. S. M. Khyal, and A. A. Abdelghani, "Serum malondialdehyde as a lipid peroxidation marker in multiple sclerosis patients and its relation to disease characteristics", *Multiple Sclerosis and Related Disorders*, vol. 51, p. 102941,2021.

[29] W. W. Daniel and C. L. Cross, *Biostatistics: a foundation for analysis in the health sciences*. Wiley, 2018.

[30] R. M. Silverstein and G. C. Bassler, "Spectrometric identification of organic compounds", *Journal of Chemical Education*, vol. 39, no. 11, p. 546,1962.

[31] S. M. Al-Majidi and M. G. Al-Khuzaie, "Synthesis and Characterization of New Azo Compounds Linked to 1, 8-Naphthalimide and Studying Their Ability as Acid-Base Indicators", *Iraqi Journal of science*, vol. 60, no. 11, pp. 2341-2352,2019.

[32] A. Daina and V. Zoete, "A BOILED-Egg To Predict Gastrointestinal Absorption and Brain Penetration of Small Molecules", *ChemMedChem* vol. 11, no. 11, pp. 1117-1121,2016.

[33] C. A. Lipinski, F. Lombardo, B. W. Dominy, and P. J. Feeney, "Experimental and computational approaches to estimate solubility and permeability in drug discovery and development settings", *Advanced Drug Delivery Reviews*, vol. 46, no. 1, pp. 3-26,2001.

[34] A. Al-basheer and S. Al-wandawi, "In vitro assessment of the antioxidant and antitumor potentials of biogenic silver nanoparticle", *Iraqi Journal of Science*, vol. 61, no. 6, pp. 1253-1264,2020.

[35] A. Menzel, H. Samouda, F. Dohet, S. Loap, M. S. Ellulu, and T. Bohn, "Common and Novel Markers for Measuring Inflammation and Oxidative Stress Ex Vivo in Research and Clinical Practice-Which to Use Regarding Disease Outcomes?", *Antioxidants*, vol. 10, no. 3, pp. 414-476,2021.